

ABSORPTION MEASURE DISTRIBUTION IN MRK 509

T. P. ADHIKARI¹, A. RÓŻAŃSKA¹, M. SOBOLEWSKA^{1,3} AND B. CZERNY²*Accepted for publication in Astrophysical Journal*

ABSTRACT

In this paper we model the observed absorption measure distribution (AMD) in Mrk 509, which spans three orders of magnitude in ionization level with a single-zone absorber in pressure equilibrium. AMD is usually constructed from observations of narrow absorption lines in radio-quiet active galaxies with warm absorbers. We study the properties of the warm absorber in Mrk 509 using recently published broad-band spectral energy distribution observed with different instruments. This spectrum is an input in radiative transfer computations with full photoionisation treatment using TITAN code. We show that the simplest way to fully reproduce the shape of AMD is to assume that the warm absorber is a single zone under constant total pressure. With this assumption we found theoretical AMD which matches the observed one determined on the basis of 600 ks RGS XMM-Newton spectrum of Mrk 509. The softness of the source spectrum and the important role of the free-free emission breaks the usual degeneracy in the ionization state calculations, and the explicit dependence of the depths of AMD dips on density open a new path to density diagnostic for the warm absorber. In Mrk 509 the implied density is of the order of 10^8 cm^{-3} .

Keywords: instabilities - radiative transfer - method: numerical - galaxies: active - galaxies: individual: Mrk 509

1. INTRODUCTION

There is a general consensus based on high resolution X-ray data that the majority of the Seyfert galaxies contain ionised absorbing gas in their line of sight. After the advancements in the observing X-ray instrumentation as *Chandra*, *XMM-Newton*, *Suzaku*, the extensive studies of the Warm Absorber (hereafter WA) in AGN were performed. Many narrow absorption lines from highly ionised elements, detected with the use of gratings, provided a great opportunity to study this warm material; (Kaspi et al. 2001; Collinge et al. 2001; Kaastra et al. 2002; Behar et al. 2003; Netzer et al. 2003; Krongold et al. 2003; Yaqoob et al. 2003; Steenbrugge et al. 2003; Blustin et al. 2003; Róžańska et al. 2004; Turner et al. 2004; Steenbrugge et al. 2005; Costantini et al. 2007; Winter & Mushotzky 2010; Winter et al. 2012; Tombesi et al. 2013; Laha et al. 2014, and many other papers).

Some physical parameters of WA were estimated, but some are still difficult to constrain. From energy shifts of line centroids, it was found that the absorbing matter is systematically outflowing with velocities in the range $10^2 - 10^3 \text{ kms}^{-1}$ (Kaspi et al. 2001; Kaastra et al. 2002). Directly from observations, ionic column densities of particular ions could be found and they are typically of the order of $10^{15} - 10^{18} \text{ cm}^{-2}$. In the next step, by assuming separate ionisation zone for each ion, it is possible to calculate the equivalent hydrogen column densities, knowing ion's ionisation fraction from photoionisation codes such as CLOUDY, XSTAR, SLAB, XABS. Such equivalent hydro-

gen column densities are in the range of $10^{18} - 10^{22} \text{ cm}^{-2}$ (Steenbrugge et al. 2005; Costantini et al. 2007). Moreover, those densities correspond to the continuous change of ionization parameter ξ (see Eq. 1 for definition), which spans the range of a few decades, $\log(\xi) \sim -1$ up to 4.

Since then, several attempts have been made to model continuous ionisation structure of the WA in several AGN (Holczer, Behar & Kaspi 2007; Behar 2009; Detmers et al. 2011). Furthermore, Holczer, Behar & Kaspi (2007) proposed to describe ionisation structure of the wind by showing absorption measure distribution (AMD) obtained by a derivative formula (Eq. 5 in this paper). These authors, for the first time, have shown that in the case of the source IRAS 13349+2438, AMD obtained from observations has deep minimum in column density that is consistent with the negligible absorption of gas with $\log(\xi)$ between 0.8 and 1.8. Such deep minima are present in AMD of other objects as well (see for instance Behar 2009; Detmers et al. 2011; Stern et al. 2014), and they are interpreted as the observational evidence for thermal instability in a given ionisation and the temperature regime.

To reproduce the observed AMD theoretically, we should consider continuous ionisation structure of WA in such a way that we can obtain proper normalisation of the AMD function. It has been done recently by Stern et al. (2014) assuming a radiation pressure confinement (hereafter RPC) of the WA material. The authors considered that the WA consists of the stratified clouds, for which P_{gas} increases gradually with decrease of P_{rad} . The exponential decrease of the radiation pressure is caused via absorption on the material when the distance from the illuminating source, i.e. active nucleus, gradually increases. The authors were successful in reproducing the normalisation and the slope of AMD for Sy1 galaxies by showing the comparison of the model with observational points of AMD for the six best studied sources. Nevertheless, they were not able to quanti-

tek@camk.edu.pl

¹ Nicolaus Copernicus Astronomical Center, Polish Academy of Sciences, Bartycka 18, 00-716, Warsaw² Center for Theoretical Physics, Polish Academy of Sciences, Al. Lotnikow 32/46 02-668, Warsaw³ Harvard-Smithsonian Center for Astrophysics, 60 Garden Street, Cambridge, MA 02138, USA

tatively reproduce the deep minimum in column density for those six objects present in the $\log \xi$ between 0.8 and 2.

In this paper, we show how AMD for the Sy1.5 galaxy Mrk 509 can be successfully reproduced by the WA being under the condition of constant total pressure, which is a sum of gas and radiation pressure (Rózańska et al. 2006; Gonçalves et al. 2006). The radiation pressure is computed from the radiation field at each point of the computations and it is added to the gas pressure. We neglect other pressure components, for instance the magnetic one. We used the broad band spectral energy distribution of Mrk 509 from the paper of Kaastra et al. (2011) (hereafter K11) to represent the radiation illuminating the WA cloud. Assuming the plane parallel geometry, we carried the simulations using TITAN photoionisation code (Dumont, Abrassart & Collin 2000). By assumption of constant total pressure, the matter of the WA is self consistently stratified without any additional requirements. The decrease of the radiation pressure is self consistently computed within photoionisation code TITAN and occurs due to absorption and emission i.e. all possible interactions of radiation field with matter. Since exact radiative transfer is computed, radiation pressure self consistently influences the matter structure. For the differences between escape probability mechanism and exact radiative transfer calculations we refer readers to the paper by Dumont et al. (2003).

Since the radiation field influences the matter structure and eventual thermal instabilities, S-curve, which is the dependence of the temperature T on the dynamic ionisation parameter Ξ (Eq.2 for definition), can be fully constructed with the use of a single cloud and with TITAN calculations (Rózańska et al. 2006). In this paper, we compare results obtained with two codes, TITAN and CLOUDY, for exactly the same physical input: spectral energy distribution (SED) of Mrk 509 as the incident radiation. The two codes differ in the way they treat the radiative transfer, and only with the use of TITAN we managed to compute thermally unstable regions and fully reproduce deep minima in the observed AMD of Mrk 509 (Detmers et al. 2011).

This result is a direct proof that thermal instabilities are responsible for the deep minimum in the column densities of AMD. Moreover, it provides strong evidence that the WA in AGN is compressed by radiation pressure, and it should be modelled with proper treatment of this effect.

The overall structure of the paper is as follows: section 2 contains the information about the incident radiation shape we used in photoionisation calculations. The description of the photoionisation codes and results of the photoionisation calculations are given in section 3. In section 4, we present the method of determining AMD from observations and calculating AMD from our models. Finally, we compare our theoretical AMD with the observational data. The conclusions are presented in section 5.

2. MRK 509 AND ITS SPECTRAL SHAPE

Mrk 509 with redshift of 0.034397 (Huchra et al. 1993), is one of the best studied local AGN, with exceptionally high luminosity $L(1-1000 \text{ Ryd}) = 3.2 \times 10^{45} \text{ erg s}^{-1}$ classified as a Sy1 galaxy. Usually it is considered to be one

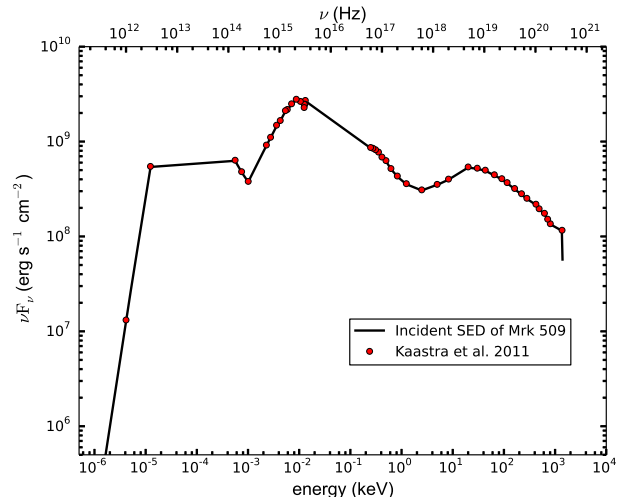


Figure 1. Spectral energy distribution of Mrk 509. The black line corresponds to the incident spectrum which is the input to the photoionisation codes TITAN and CLOUDY (see text for explanation). The red circles are the points adapted from K11 and normalised to incident flux at the corresponding inner radius of the cloud.

of the closest QSO/Sy1 hybrids. Peterson et al. (2004) have reported that Mrk 509 harbours a super massive black hole of mass $1.4 \times 10^8 M_{\odot}$.

The WA in this source was extensively studied with 600 ks RGS (reflection grating spectrometer) on board of *XMM-Newton* X-ray telescope (Detmers et al. 2011; Kaastra et al. 2012). The few tens of absorption lines from highly ionized metals were identified, allowing for determination of ionic column densities. Furthermore, equivalent hydrogen column densities were calculated for each ion, and absorption measure distribution was constructed (Detmers et al. 2011). Additionally, the upper limits on the location of different ionisation phases of the WA were estimated, using the variability method, which requires the assumption that any observed changes are caused by changes in the ionisation states (Kaastra et al. 2012). Those authors reported that observed ionisation components span the distance upper limits from 5 to 400 pc.

For any consistent photoionisation calculations of WA, the broad-band spectral energy distribution of the source is crucial. It was shown by Rózańska, Kowalska & Gonçalves (2008) that if SED of an AGN is dominated by a soft component (i.e. an accretion disk), the stability curve obtained during photoionisation calculations differs substantially from that obtained with the AGN SED dominated by a hard X-ray power-law component. The authors also explained that this is due to the fact that in the case of soft radiation entering the WA, bremsstrahlung is the dominant cooling in the cloud, while in the case of hard X-ray illumination, Compton scattering is responsible for high temperature equilibrium in the WA. A systematic study of how the stability curve depends on the shape of the incident SED was done by Chakravorty et al. (2009). In particular, the authors discussed the influence of the soft X-ray excess on the shape of the stability curve in this paper. Additionally, chemical abundances affect the ionisation balance of the WA (Hess, Kahn & Paerels 1997),

and hence also the shape of the resulting stability curve. Nevertheless, for this paper we assume Solar chemical abundances, and we keep them constant during all photoionisation calculations.

Recently, very detailed observed continuum spectral shape of Mrk 509 was published by K11. The spectrum was obtained during their multi-wavelength campaign of several observations taken in various energy bands, with *XMM Newton*: RGS, EPIC (pn, MOS), and OM. Simultaneously with *XMM-Newton* observations, data with *INTEGRAL* was also obtained to observe the hard X-rays. Additionally, they collected the data of Mrk 509 with *Chandra* LETGS together with *HST* COS UV detection. Moreover, observation of Mrk 509 was done with *Swift*, using both the instruments: XRT and UVOT. For the final construction of SED, the authors used IR points from *IRAS* and *Spitzer* data, but it is unclear how much of IR emission is seen by the outflow. This is because most probably the wind is located closer to the black hole than the dusty torus from which most the IR radiation is originated.

K11 allowed us to use those points for our project. The SED of Mrk 509 covers a wide range of wavelength band, which is essential for obtaining the ionisation balance needed for photoionisation modelling. All observed spectral points are presented in Fig. 1 as red circles. Mrk 509 has one of the best spectra covering broad band among all the well studied AGN. Black line on the same figure demonstrates the incident SED used by us in photoionisation calculations by TITAN and CLOUDY code. Both codes allow for the input of incident spectrum by points and the linear interpolation is done in order to fully define incident continuum which goes into the simulations.

3. PHOTOIONISATION CALCULATIONS

Here, we study the detailed structure of the WA cloud using the photoionisation codes TITAN (Dumont, Abrassart & Collin 2000) and CLOUDY 13.02 (Ferland et al. 2013) with the same initial physical conditions. Although both codes are used to study the clouds subjected to the incident radiation emanating from the central source, they do differ in their assumptions of radiative transfer treatments and number of spectroscopic lines considered. Nevertheless, the general idea is the same. Both codes solve radiation transfer through the gas in thermal and ionisation equilibrium with non-LTE equation of state.

The most important difference between codes is that CLOUDY uses escape probability mechanism to solve radiative transfer, while TITAN uses Accelerated Lambda Iteration (ALI) method (Collin, Dumont & Godet 2004), which is more accurate in optically thick media. The detailed comparison of both radiative transfer methods in the context of X-ray absorbing gas was done in Dumont et al. (2003). Below, we show and compare the output of two codes in the case of our particular source Mrk 509 and its warm absorber.

Following assumptions are made for this modelling in both photoionisation codes. The geometry of the cloud is set to the plane parallel. The expression for the ionisation parameter ξ , at the irradiated surface of the cloud relating to the distance from the illuminating source R

is:

$$\xi = \frac{L_{\text{ion}}}{nR^2} \quad (1)$$

where L_{ion} is the luminosity of the ionising source and n is the hydrogen number density. The luminosity can be obtained from observations, whereas the number density and ionisation parameter are free parameters in our calculations.

3.1. TITAN computations

TITAN was developed by Dumont, Abrassart & Collin (2000) and was mainly designed to determine the structure of temperature and ionisation state and the continuum emission spectrum of a thick hot photoionised slab of gas. Using this code, the physical state of the gas is computed at each depth, assuming the local balance between ionisation and recombination of ions, excitation and deexcitation, local energy balance and finally total energy balance. TITAN assumes the transfer of both continuum and lines using ALI method, which precisely computes line and continuum intensity self consistently. There are many options to control the physical properties of the absorbing gas. Here, to calculate the stability curve which is compared to CLOUDY code (Sec. 3.3), we use the assumption of constant density slab, but for the explanation of AMD in Mrk 509 we reject this assumption and compute more realistic constant total pressure cloud (see results in Sec. 4). This exercise is made to ensure the reader, that stability curves calculated by both codes agree for the same physical conditions of the gas.

For the purpose of this paper, we make stronger assumption that the total pressure (i.e. gas and radiation pressure: $P_{\text{gas}} + P_{\text{rad}}$) is held constant throughout the plane parallel slab of the gas, and the volume density and ionisation parameter across the cloud are stratified. The assumption of constant pressure allows the ionised gas to be naturally stratified due to illumination, as discussed in (Róžańska et al. 2006). The computations of all the structure are done iteratively until the convergence is reached.

In the constant total pressure model, plane parallel geometry is considered, and the radiation source is assumed to hit the cloud perpendicular to the surface. The parameters of the model are the ionisation parameter ξ_0 , and the hydrogen number density n_0 (both defined at the illuminated cloud surface), the total column density N_H , and the incident SED. Although the ionisation parameter is well constrained in the surface of the illuminated cloud, ionisation properties are continuously changing as we go deeper into the cloud. This happens since all thermodynamical parameters such as: gas temperature, gas density, and the radiation pressure do change with the depth of the cloud. To trace this behaviour, the dynamic ionisation parameter, Ξ is defined as:

$$\Xi = \frac{\xi}{4\pi ckT} = \frac{L_{\text{ion}}}{4\pi cR^2} \frac{1}{nkT} = \frac{F_{\text{ion}}}{cP_{\text{gas}}} = \frac{P_{\text{rad}}}{P_{\text{gas}}} \quad (2)$$

where F_{ion} is a flux affecting the cloud, c is a velocity of light and T is the temperature of the gas. Here, we do not follow the standard convention that P_{gas} accounts only for hydrogen density number n . For fully ionised gas, with heavy element abundance, the total density

number equals $\approx 2.3n$, and if the gas pressure is computed with total density, the factor 2.3 should be taken into account, as it is in the basic definition of Ξ , given by Krolik, McKee & Tarter (1981). Nevertheless, since the observers do not use the value of density while determining AMD from observations, we compute the current value of ξ using temperature, radiation pressure and the gas pressure, which directly comes out from our code.

All thermodynamical parameters describing the cloud structure as temperature, radiation pressure, hydrogen and total density numbers are given as functions of the distance from illuminating source. Therefore, we can self consistently compute both ionisation parameter and its change with the distance from the cloud illuminated surface, using the value of radiation pressure computed from the second moment of radiation field.

3.2. CLOUDY computations

CLOUDY is a well documented public code extensively used in the calculation of the photoionisation in many different clouds surrounding planetary nebulae, in the interstellar medium and Active Galaxies. It has an extensive explanation of the physics of the plasma subjected to different perturbations given in the well organised books: (Hazy1 and Hazy2)⁴. The same as in TITAN runs for CLOUDY calculations, we assumed the open geometry with thin plane parallel zones. All other input parameters as: the incident SED, the ionisation parameter, the inner radius, the total column density of the slab and the hydrogen density at the surface of the illuminated cloud are the same in both codes. We did this simulation for many grids of densities. The default option in the CLOUDY is the constant density through the cloud. Nevertheless, there is an option to calculate cloud under constant pressure, and we check it and discuss in this paper.

3.3. Stability curves for constant density clouds

The general way for the analysis of the stability of the cloud subjected to the incident radiation from the central source is to study a stability curve, i.e. temperature as a function of the ratio of the radiation pressure to the gas pressure, which is a dimensionless parameter Ξ (Eq. 2). Such defined stability curve can be computed in several ways. The most natural way is to compute a grid of constant density clouds located at the same distance from the illuminated source. By changing the cloud density, we change the ionisation parameter and so the gas temperature of the cloud. In Fig. 2, we compare stability curves computed in this way by two photoionisation codes CLOUDY (cyan triangles), and TITAN (magenta squares). Both codes use parameter selection of the clouds tabulated in Table 1. For each calculation, we considered the source luminosity 3.2×10^{45} ergs s⁻¹ and the inner radius of the cloud, i.e., the distance between the source and the illuminated face of the cloud is taken as $\log(r_0/\text{cm}) = 17.25$.

In case of extended envelopes, the radiation pressure changes while we go deeper into the cloud due to geometrical dilution and absorption by ionised gas. Therefore, in principle, it is possible to calculate extended, spheri-

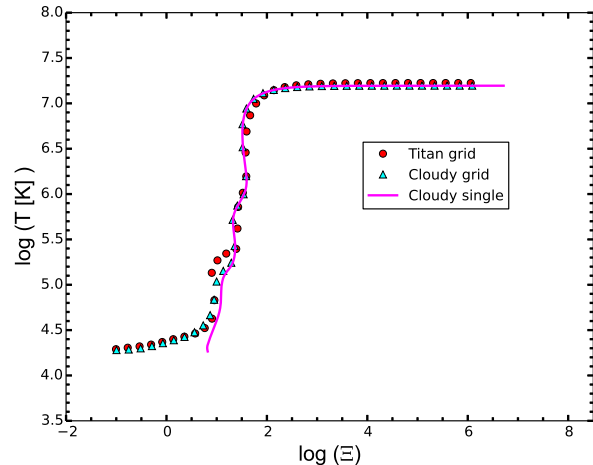


Figure 2. Equilibrium S-curves for constant density plane-parallel clouds obtained with the photoionisation codes TITAN magenta circles, and CLOUDY cyan triangles. Additionally, constant density single cloud with $n_H = 1$ in spherical geometry computed with CLOUDY is presented by solid magenta line.

Table 1

Constant Density Cloud parameters. When the range of densities is shown that means the grid of clouds were calculated. The inner cloud radius in all cases is $\log(r_0/\text{cm}) = 17.25$.

Codes Used	n_0 (cm ⁻³)	ξ_0 (ergs cm s ⁻¹)	Geometry
TITAN	10 ² -10 ¹²	as L/nr^2	plane parallel
CLOUDY	10 ² -10 ¹²	as L/nr^2	plane parallel
CLOUDY	1	10 ¹¹	Spherical

cally symmetric cloud at constant density. While entering deeper inside the cloud, the luminosity decreases as a distance square, and ionisation parameter of the consecutive zone decreases. A full stability curve can be reconstructed also in this way, as presented in Fig. 2 by magenta solid line.

All curves agree for temperatures down to 3×10^4 K. Below this temperature, atomic data which are different in the two codes may cause some inconsistencies. But since we concentrate here on the warm absorbers, we may consider that both codes work perfect in the considered temperature regime.

3.4. Stability curves for constant pressure clouds

As shown in Fig. 3, the constant pressure stability curves from TITAN and CLOUDY shows the similar trend except for the considerable difference in the thermal instability zone. Thermal instability zones are part of the stability curve where the slope is negative. The main difference between two codes here is that CLOUDY is not able to compute the structure at the zones of instability (there are no points on the unstable branch of stability curve). The stability curve computed by TITAN shows several points on unstable branch. Also there is a difference in the range of ionisation parameter at which the instability occurs. Such difference may be due to the different approximations used in the code to solve thermal balance equation and the differences in the atomic database used.

⁴ <http://nublado.org/>

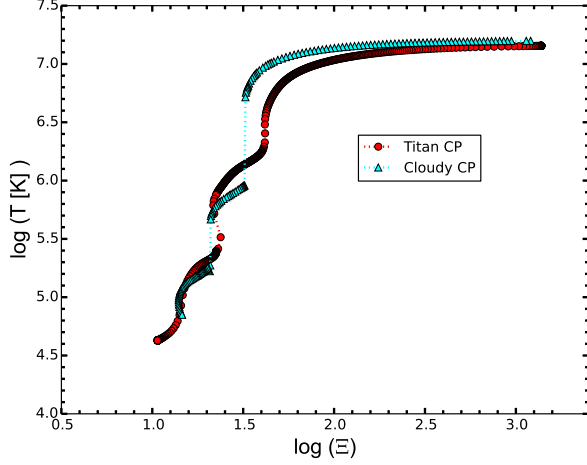


Figure 3. Equilibrium S-curve obtained from CLOUDY (red) and TITAN (cyan). Both curves are produced with the number density $n_0 = 10^6 \text{ cm}^{-3}$ and ionisation parameter $\xi = 10^6 \text{ erg cm s}^{-1}$ at the irradiated surface of the cloud. The inner radius to the cloud is set to $\log(r_0/\text{cm}) = 16.75$ cm, to ensure that illuminating luminosity is equal to the observed one. The total column density (N_H) of the slab in both calculation is set to $1.5 \times 10^{23} \text{ cm}^{-2}$.

4. ABSORPTION MEASURE DISTRIBUTION

The distribution of the absorbing column in the line of sight is often described as Absorption Measure Distribution (AMD). Almost always the large range or ionisation state of gas located on the line of sight towards observer is seen in AGN with the warm absorber. A few tens of absorption lines is detected in high resolution spectra of several AGN. Each line can be treated as an constant density absorber and using photoionisation code for the thin slab, we can calculate the ionisation parameter and ionic column density N_{ion} of the slab required to produce such an observed absorbing feature. Holczer, Behar & Kaspi (2007) formulated the expression for quantifying the strength of absorption at these different ionisation states as:

$$\text{AMD} = \frac{dN_H}{d(\log \xi)} \quad (3)$$

where, ξ is defined by Eq. 1, and N_H is the total hydrogen column density along the line of sight. Furthermore, if solar abundances A_{Z_\odot} are assumed, the equivalent hydrogen column density can be calculated separately for each ion using relation:

$$N_H \approx \frac{N_{\text{ion}}}{f_{\text{ion}}(\xi_{\text{max}}) A_{Z_\odot}}, \quad (4)$$

where $f_{\text{ion}}(\xi_{\text{max}})$ is the fractional ion abundance with respect to the total abundance of its element, and ξ_{max} is the maximum value of ionisation parameter required to produce the observed feature. In nature there is a distribution of gas with different ξ , which may account for absorption in the line, and in reality one must take into account the full dependence of f_{ion} on ξ . This means that when ionic column densities for individual warm absorber are measured, the AMD can be derived from

the formula:

$$N_{\text{ion}} = A_{Z_\odot} \int \text{AMD} f_{\text{ion}}(\log \xi) d(\log \xi). \quad (5)$$

It is not possible to get the hydrogen column density directly from observation since we do not see hydrogen lines. It is derived using the ionic column densities of each ions assuming continuous distribution of the absorbers for several objects, including Mrk 509 (Detmers et al. 2011). It should be noted that the hydrogen column densities derived from the observations are nominal and model dependent. For instance, in Detmers et al. (2011) paper, authors always used thin slabs, assuming that lines are unsaturated. Even adding the thin slabs together authors make a strong assumption that they are on the linear part of the curve of growth, and the fitted ionic column densities are always only lower limits. This kind of analysis is valid if the absorber is optically thin. For optically thick lines, the absorber can possess higher column density with the same strength of saturated lines. As a result the normalization of AMD fitted by thin slabs can be underestimated by one order of magnitude. Below, we present the modelled AMD, computed from the gas with continuous distribution of ionisation parameters, as a result of the constant total pressure balance.

4.1. Modelled AMD for Mrk 509

We used the TITAN photoionisation code to reproduce AMD for Mrk 509 assuming that the absorbing cloud is in total pressure equilibrium (Rózańska et al. 2006). When a cloud is irradiated with the incident SED of the source, the total pressure equilibrium requirement self consistently provides the distribution of the ionization parameters for which the AMD is calculated. Note, that when we compute AMD from simulations, we compute ξ at each depth by relation:

$$\xi = 4 \pi c k T \frac{P_{\text{rad}}}{P_{\text{gas}}(H)} = 4 \pi c \frac{P_{\text{rad}}}{n}. \quad (6)$$

Our model of constant pressure reproduces the AMD derived observationally by Detmers et al. (2011). Both discontinuities seen in the distribution of AMD in their paper are reproduced using our model. We made several exercises how the AMD behaves with different parameters and the results are as follows.

For the detail investigation of the effect of the density on AMD structure, we made several runs with densities $n_0 = 10^5, 10^6, 10^8$ and 10^9 cm^{-3} as presented in Fig. 4 (the density $n_0 = 10^7 \text{ cm}^{-3}$ is removed from the figure for clarity). For lower values of the density at the illuminated face of cloud n_0 upto 10^8 cm^{-3} , the position of the dips remains the same. For higher densities the position of dips in AMD changes. This is connected with the fact reported by Rózańska, Kowalska & Gonçalves (2008) that photoionisation models with high density similar to those in Broad Line Region (BLR) are not degenerated any more when SED of central source is dominated by strong optical/UV component. This is a case of Mrk509. The physical reason for this is that in the case of the hard incident spectrum all radiative processes (Comptonization, line heating/cooling) are linear

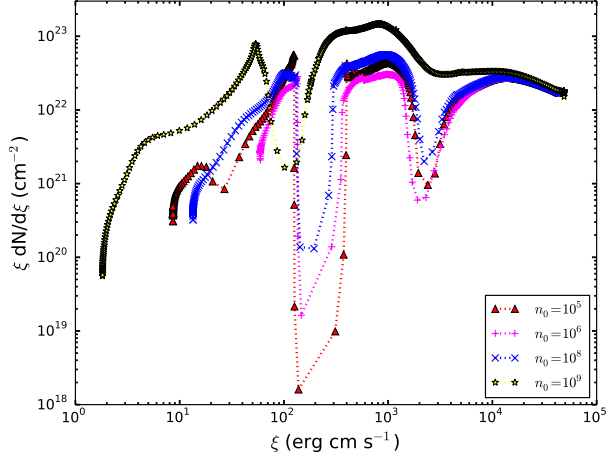


Figure 4. AMD structure for the same initial ionisation parameter $\xi_0 = 4.3 \times 10^4 \text{ erg cm s}^{-1}$ and different number densities at illuminated side of clouds marked in right bottom corner.

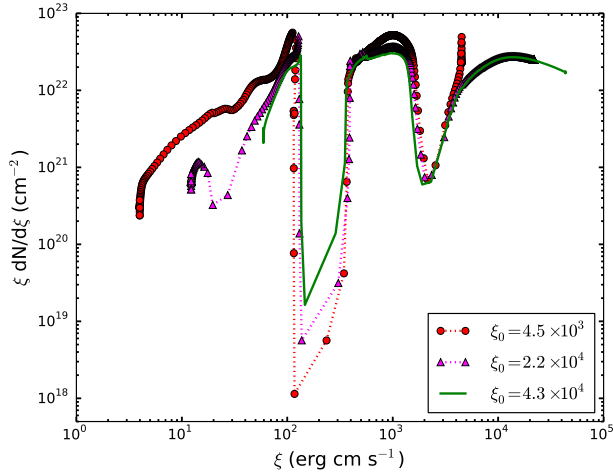


Figure 5. AMD structure for the same initial number density $n_0 = 10^6 \text{ cm}^{-3}$ and different values of ionisation parameters at illuminated side of clouds marked in left upper corner.

in density and the solution is determined by the ionization parameter, independently from the local density. However, for soft incident spectra the bremsstrahlung plays an important role, and the quadratic dependence of the bremsstrahlung (free-free) on the density breaks the degeneracy and introduces a dependence on the density (Róžańska, Kowalska & Gonçalves 2008).

As can be seen from the Fig. 4, when the densities are comparable to the Narrow Line Region (NLR) densities, the two dips remain prominent almost around the same range of ionisation states. As we move towards the regime where the density is comparable to the BLR density, i.e. at $n_0 = 10^9 \text{ cm}^{-3}$, there is only one prominent dip present. Computations for higher densities show only one dip in AMD, but the amount of material in the absorber produces much higher normalization of the modelled AMD than it is observed. It is difficult to say if the disappearance of this dip is connected with a switch in radiative cooling as it is valid in photoionisation models

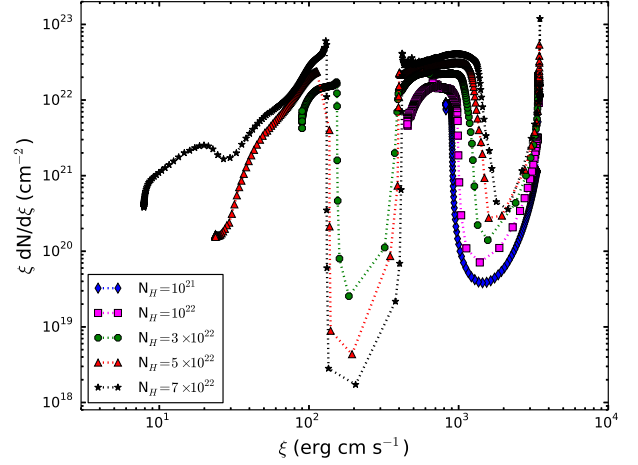


Figure 6. AMD structure for the same SED and different values of total column density considered. This is a case with $n_0 = 10^8 \text{ cm}^{-3}$ and $\xi_0 = 3.4 \times 10^3 \text{ erg cm s}^{-1}$. Absorbers with low column densities, less than 10^{22} cm^{-2} , do not have enough matter to pass through two dips in AMD distribution. Those cases are indicated by blue diamonds and magenta squares.

of different density. The line cooling may also be important. To confirm this result, the different SED should be considered and we plan to explore this problem in the future work.

Overall normalization of the AMD does not change much for densities up to 10^8 cm^{-3} , but the normalization of dips is different. Dips are deeper for lower incident densities of the absorber. The depths of the two dips were the main criteria used in our comparison of modelled to the observed AMD presented below in Sec. 4.2.

In Fig. 5, we show the dependence of the AMD structure on the initial ionisation parameter at the irradiated side of the absorber, ξ_0 . It can be seen that the location of the instability region remains at the same ionization range inside the absorber. The difference is only in the normalisation of the dips.

There is no difference in absorption measure distribution from the clouds of the same density affected by various luminosities if we assume the same ionization parameter. This is obvious due to the fact that for the same product of ξn_H the same energy flux L/R^2 is illuminating the absorber.

We also investigated the effect of different total column densities of the cloud on AMD. It is shown in Fig. 6 and Fig. 7 for the number densities $n_0 = 10^8 \text{ cm}^{-3}$ and $n_0 = 10^9 \text{ cm}^{-3}$ respectively at the illuminated side the of the absorber. As we can see from the Fig. 6, absorbers at lower total column density do not give two dips in AMD. Also their overall normalization is lower by about the half order of magnitude. If the total column density is higher than 10^{22} cm^{-2} , the AMD has always two dips. The absorption measure distribution ends at lower ionization parameter for higher total column density of the constant pressure cloud. As seen in Fig. 7, when the column density is substantial, further increase of this parameter does not change the distribution of AMD dips. This result is consistent with the conclusion made by Stern et al. (2014).

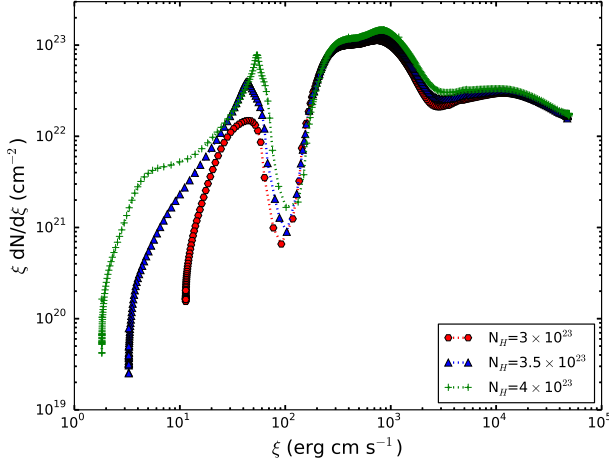


Figure 7. AMD structure for the same SED and different values of total column density considered. This is a case with $n_0 = 10^9 \text{ cm}^{-3}$ and $\xi_0 = 4.3 \times 10^4 \text{ erg cm s}^{-1}$.

4.2. Comparison with observations

The direct comparison of an observed AMD with the modelled one is quite hard. This is because, for the given source we do observe only from several to several of tenth of absorption lines. Each line puts a point on AMD as described in the beginning of Sec. 4. Note, that in case of computed models, a few thousands of lines are included, therefore AMD has many more points.

To date, observed AMD are found from individual observations of several objects. The general behaviour of AMD in case of five Sy1 galaxies was given by Behar (2009). All of those five galaxies: NGC 3783, NGC 5548, MCG-6-30-15, NGC 3516, NGC 7469, IRAS 13349+2438, reveal one dip in AMD located more or less in the same place between $\log \xi = 0.8 - 2$. The dip is not explained by RPC model presented in this paper. Additionally those objects are rather Sy1 galaxies with different SED than Mrk 509. The illuminating SED has the strong influence on AMD. For Sy 1.5 galaxy Mrk 509, AMD reveals two dips as shown by Detmers et al. (2011).

The comparison between the observed AMD for Mrk 509 (Detmers et al. 2011) and our constant pressure model computed with realistic SED input taken from current multi-wavelength studies (K11) is shown in Fig. 8, where observations are given by black histogram, and red triangles describe our model. Our calculations show the distribution of the ionization parameter much more densely. Furthermore, our column density presented in the figure by red triangles is the realistic column density, with radiation transmitted through all zones in the sequence, instead of transmission through a collection of independent zones, as in data modelling by (Detmers et al. 2011), as given above by Eq. 5. The lower panel of Fig. 8 shows absolute values of AMD normalization. It is obvious that modelled normalization is by an order of magnitude higher than the observed one in the stable zones. In the upper panel, we re-scale the normalization to show that dips are fully reconstructed by our model for the given incident density and ionization parameter. We argue here, that the difference in the normalization occurs, since observed lines are saturated. Therefore, the derived

ionic column densities from observations using thin slabs give only lower limits, and in reality can be one order of magnitude higher. To check our prediction we have to use saturated models to fit the data. They are not very common in the literature.

There are few values of AMD normalization of several objects reported in the recent papers both from observation and modelling. Summarizing, the agreement in the overall shape of the modelled and observed AMD dependence on the ionization parameter is very encouraging but the normalization of the measured and modelled AMD remains as an issue. The observed AMD normalization of Mrk 509 corresponding to the ionization parameter $\xi = 8 \times 10^2 \text{ erg cm s}^{-1}$ is $\sim 10^{21} \text{ cm}^{-2}$ (Detmers et al. 2011), less by a factor of ~ 30 than the AMD normalization from our best fitted constant total pressure model with TITAN ($\sim 3 \times 10^{22} \text{ cm}^{-2}$). The AMD modeled by Stern et al. (2014) within the frame of their RPC model were shown to be fairly universal, only weakly dependent on the model parameters, and the obtained normalization values were $\sim 1.1 \times 10^{22} \text{ cm}^{-2}$. Measurements of AMD in six other objects (Behar 2009) implied values of the order of $\sim 4 \times 10^{21} \text{ cm}^{-2}$. Thus modelled values of AMD normalizations are frequently higher than the observed ones, and it is not clear whether the problem lies in the measurement method or in the modelling.

Nevertheless, for the first time, the AMD dips can be shown in model computations. The discontinuities in AMD distribution are in the range of the ionisation parameter, $\log \xi = 2 - 3$ and $\log \xi = 3 - 4$. These ranges of ξ corresponds to the ranges of temperatures $T = (4 - 9) \times 10^5$ and $T = (2 - 5) \times 10^6 \text{ K}$, presented in Fig. 9 by the green solid line. This is a proof that the absorbing material should be in pressure equilibrium and thin thermally unstable regions can be clearly visible. This comparison clearly shows that the warm absorber in Mrk 509 is the continuous cloud under constant total pressure.

The two dips are the result of the thermal instability operating in the irradiated medium. To show this effect we present the structure of main cloud parameters as the gas pressure, temperature, density and the ionisation parameter ξ as the function of column density in Fig. 9. We show the plot of total cross section (σ_{tot}) versus column density in Fig. 10 for the same case of cloud as in Fig. 9. Two cases of a sudden rise of the total cross section and a drop in the temperature can be clearly noticed, and we argue that they are responsible for the two dips in the observed AMD for Mrk 509. The discontinuity is not well resolved in the radiative transfer codes. As it was pointed out by Róžańska & Czerny (1996) thermally unstable zones are geometrically very thin and the correct temperature profile in the transition zone can be recovered only after including the electron conduction. Neither TITAN nor CLOUDY have this option. However, the position of the discontinuity is well determined on the basis of radiative transfer only, as was shown by Czerny et al. (2009) and its extension depends on the model parameters.

Our result puts strong constraints that the warm absorber is build from the material of the density of the order of 10^8 cm^{-3} . For SED observed in Mrk 509, the value

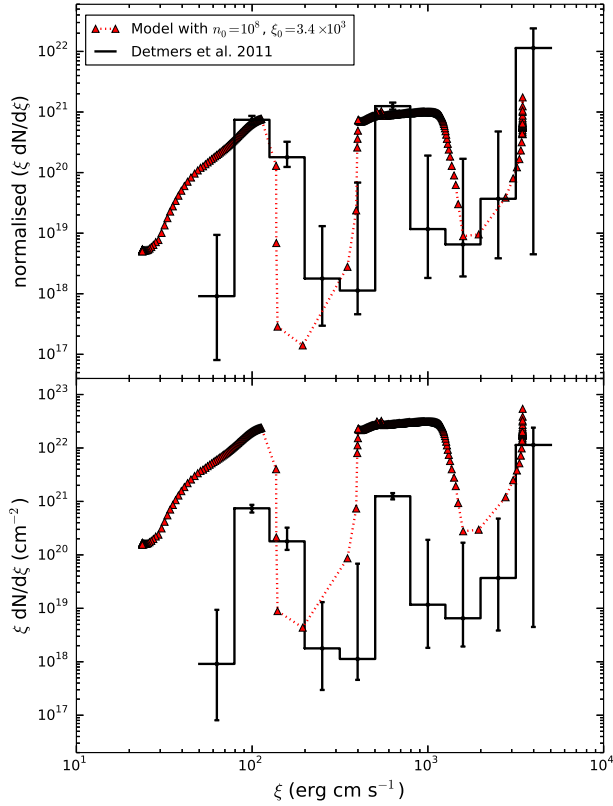


Figure 8. The comparison of the simulated AMD structure - red triangles, with the observed one - black histogram. Data and error bars are taken from the paper by Detmers et al. (2011). The best model which roughly matches the data is computed for $n_0 = 10^8 \text{ cm}^{-3}$, $\xi_0 = 3.4 \times 10^3 \text{ erg cm s}^{-1}$ and $L = 3.2 \times 10^{45} \text{ erg s}^{-1}$. Bottom panel presents data with absolute normalization, while in the upper panel the modelled AMD is scaled down by a factor ~ 30 to match the observed points on the stable branch. The best fit model represents well the depth of the two dips.

of density changes the nature of the AMD. For densities smaller than 10^9 cm^{-3} , we see two dips of different depth, as observed, and the best models compared to the data is for 10^8 cm^{-3} . For densities of the order of 10^9 cm^{-3} one dip for higher ionisation parameter is substantially reduced. For the given SED we were unable to converge computations for higher densities, but we plan to check it for objects from Stern et al. (2014) paper, with different shape of SEDs. Densities much lower than 10^8 lead to significant overprediction of the depth of $\xi = 200$ feature, as seen from Fig. 4. The discrepancy between the true modeled AMD normalization and the observed normalization, caused by the line saturation problems possibly broadens the acceptable density range. If indeed the stable parts of AMD are underestimated in the data, but the dips are not, the true depth of the dips should be larger than in the data. Assuming the true depth of the low ξ dip equals four decades, then the densities as low as 10^6 (but not lower) provide an acceptable solution for this part of AMD. However, the high ξ dip is then not

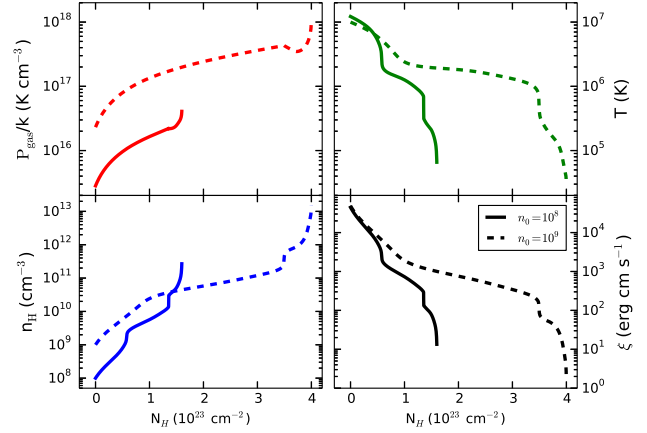


Figure 9. The structure of pressure (upper left), temperature (upper right), density number (bottom left), and ionisation parameter (bottom right), versus cloud column density for initial parameters $n_0 = 10^8 \text{ cm}^{-3}$, $\xi_0 = 4.3 \times 10^4 \text{ erg cm s}^{-1}$ (solid lines) and $n_0 = 10^9 \text{ cm}^{-3}$, $\xi_0 = 4.3 \times 10^4 \text{ erg cm s}^{-1}$ (dashed lines). In both cases illuminating luminosity is $L = 3.2 \times 10^{45} \text{ erg s}^{-1}$.

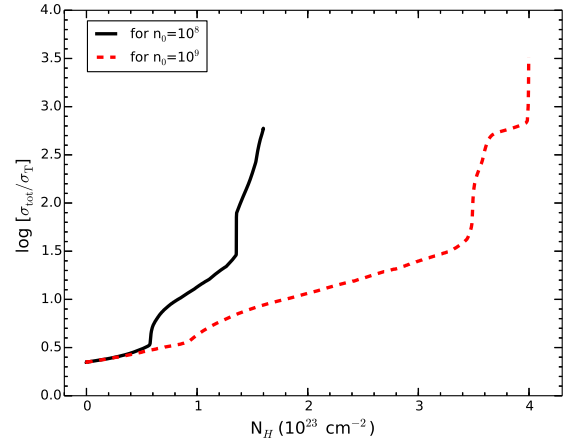


Figure 10. Total cross section (σ_{tot}) relative to Thomson cross section (σ_T) as a function of cloud column density. The initial cloud parameters are as in Fig. 9.

so well fitted.

We note, that RPC model presented by Stern et al. (2014) should reproduce the observed AMD dips since thermal instability is clearly seen in constant pressure cloud presented in Fig. 3 by cyan triangles. It was shown that CLOUDY code fully reproduces thermal instabilities under different circumstances (Rózańska & Czerny 1996; Chakravorty et al. 2012). In our opinion, the lack of AMD dip in the Stern et al. (2014) RPC model is due to the final binning of the AMD used by those authors. They have used final bins of 0.25 dex in ξ which is too rough to show thin, unstable zones. Several very small dips are actually present in the RPC model by Stern et al. (2014) (see their Fig. 2), but none of them explains observations.

5. CONCLUSIONS

We performed photoionisation simulations of the warm absorber as a cloud illuminated by the energy emitted from the AGN centre. Computations were done assuming total pressure, $P_{\text{gas}} + P_{\text{rad}}$ to be constant, and with the use of TITAN code by Dumont, Abrassart & Collin (2000).

We computed absorption measure distribution for the case of Mrk 509, for which spectral energy distribution is well known from the multi-wavelength long term monitoring. We found discontinuities in AMD in the range of the ionisation parameter, $\log \xi = 2 - 3$ and $\log \xi = 3 - 4$, similar to that obtained observationally by Detmers et al. (2011). Such observed discontinuity was often interpreted as the absence of ions in the thermally unstable regions (Holczer, Behar & Kaspi 2007), which can also be seen in the cooling curve in Fig. 3. These observed minimum is also described as two geometrically distinct regions along the line of sight representing high ionisation region and low ionisation region (Holczer, Behar & Kaspi 2007). Contrary to the work by Detmers et al. (2011), instead of two discrete zones, we explain AMD as a continuous absorber under constant total pressure.

Since the purpose of this paper is to reproduce the deep minima observed in the continuous distribution of the AMD, the modelled AMD is normalised to the observed one for convenience. The model requires higher values of column density to produce the structure all the way down to the low ionisation parameter. As a result of this, the normalisation of the modelled AMD is higher than the observed one. Nevertheless, the observed AMD are constructed with some approximations discussed in previous sections.

The model presented in this paper clearly shows that only for the warm absorber with substantial density, we can reproduce AMD in Mrk 509. We point out here, that Stern et al. (2014) did not obtain AMD dips from their RPC model since their modeled AMD was computed with too strong binning. The number of dips observed in AMD may put constraints on the density of the absorbing material, which is a crucial parameter needed to indicate the wind location through the relation Eq. 1. Our work presents new density diagnostic by matching the model with exactly the same dips normalization to the observed AMD. The dips strongly reflect geometrically narrow thermally unstable regions. For higher densities, one dip disappears for a considered SED of Mrk 509. To confirm this result and to search for a parametrization of the shape of the AMD dips in terms of the incident n_0 , it is necessary to consider a sample of sources and a range of illuminating SEDs. We plan to investigate this issue in the future work.

We are grateful to anonymous referee for extremely helpful comments. We want to thank J. S. Kaastra for providing us the spectra of Mrk 509 and AMD points, we used in our study. We thank A.M. Dumont and M. Mouchet for helpful discussion on TITAN calculations and J. Stern for useful discussion on models. This research was supported by Polish

National Science Center grants No. 2011/03/B/ST9/03281, 2013/08/A/ST9/00795, and by Ministry of Science and Higher Education grant W30/7.PR/2013. It received funding from the European Union Seventh Framework Program (FP7/2007-2013) under grant agreement No.312789.

REFERENCES

- Behar E., 2009, *ApJ*, 703, 1346
 Behar E., Rasmussen A. P., Blustin A. J., Sako M., Kahn S. M., Kaastra J. S., Branduardi-Raymont G., Steenbrugge K. C., 2003, *ApJ*, 598, 232
 Blustin A. J. et al., 2003, *A&A*, 403, 481
 Chakravorty S., Kembhavi A. K., Elvis M., Ferland G., 2009, *MNRAS*, 393, 83
 Chakravorty S., Misra R., Elvis M., Kembhavi A. K., Ferland G., 2012, *MNRAS*, 422, 637
 Collin S., Dumont A.-M., Godet O., 2004, *A&A*, 419, 877
 Collinge M. J. et al., 2001, *ApJ*, 557, 2
 Costantini E. et al., 2007, *A&A*, 461, 121
 Czerny B., Chevallier L., Gonçalves A. C., Róžańska A., Dumont A.-M., 2009, *A&A*, 499, 349
 Detmers R. G. et al., 2011, *A&A*, 534, A38
 Dumont A.-M., Abrassart A., Collin S., 2000, *A&A*, 357, 823
 Dumont A.-M., Collin S., Paletou F., Coupé S., Godet O., Pelat D., 2003, *A&A*, 407, 13
 Ferland G. J. et al., 2013, *Rev. Mexicana Astron. Astrofis.*, 49, 137
 Gonçalves A. C., Collin S., Dumont A.-M., Mouchet M., Róžańska A., Chevallier L., Goosmann R. W., 2006, *A&A*, 451, L23
 Hess C. J., Kahn S. M., Paerels F. B. S., 1997, *ApJ*, 478, 94
 Holczer T., Behar E., Kaspi S., 2007, *ApJ*, 663, 799
 Huchra J., Latham D. W., da Costa L. N., Pellegrini P. S., Willmer C. N. A., 1993, *AJ*, 105, 1637
 Kaastra J. S. et al., 2012, *A&A*, 539, A117
 —, 2011, *aap*, 534, A36
 Kaastra J. S., Steenbrugge K. C., Raassen A. J. J., van der Meer R. L. J., Brinkman A. C., Liedahl D. A., Behar E., de Rosa A., 2002, *A&A*, 386, 427
 Kaspi S. et al., 2001, *ApJ*, 554, 216
 Krolik J. H., McKee C. F., Tarter C. B., 1981, *ApJ*, 249, 422
 Krongold Y., Nicastro F., Brickhouse N. S., Elvis M., Liedahl D. A., Mathur S., 2003, *ApJ*, 597, 832
 Laha S., Guainazzi M., Dewangan G. C., Chakravorty S., Kembhavi A. K., 2014, *MNRAS*, 441, 2613
 Netzer H. et al., 2003, *ApJ*, 599, 933
 Peterson B. M. et al., 2004, *ApJ*, 613, 682
 Róžańska A., Czerny B., 1996, *Acta Astron.*, 46, 233
 Róžańska A., Czerny B., Siemiginowska A., Dumont A.-M., Kawaguchi T., 2004, *ApJ*, 600, 96
 Róžańska A., Goosmann R., Dumont A.-M., Czerny B., 2006, *A&A*, 452, 1
 Róžańska A., Kowalska I., Gonçalves A. C., 2008, *A&A*, 487, 895
 Steenbrugge K. C. et al., 2005, *A&A*, 434, 569
 Steenbrugge K. C., Kaastra J. S., de Vries C. P., Edelson R., 2003, *A&A*, 402, 477
 Stern J., Behar E., Laor A., Baskin A., Holczer T., 2014, *MNRAS*, 445, 3011
 Tombesi F., Cappi M., Reeves J. N., Nemmen R. S., Baito V., Gaspari M., Reynolds C. S., 2013, *MNRAS*, 430, 1102
 Turner A. K., Fabian A. C., Lee J. C., Vaughan S., 2004, *MNRAS*, 353, 319
 Winter L. M., Mushotzky R., 2010, *ApJ*, 719, 737
 Winter L. M., Veilleux S., McKernan B., Kallman T. R., 2012, *ApJ*, 745, 107
 Yaqoob T., McKernan B., Kraemer S. B., Crenshaw D. M., Gabel J. R., George I. M., Turner T. J., 2003, *ApJ*, 582, 105